Effect of halogen atom exchange on the thermodynamic behavior and ferroelectric properties of $[C(NH_2)_3]_4Br_2SO_4$

Marek Szafrański[1] and Andrzej Katrusiak[2]
[1]*Faculty of Physics, Adam Mickiewicz University, Umultowska 85, 61-614 Poznań, Poland*
[2]*Department of Crystal Chemistry, Adam Mickiewicz University, Grunwaldzka 6, 60-780 Poznań, Poland*
(Received 12 December 2005; revised manuscript received 22 February 2006; published 19 April 2006)

A new ferroelectric, $[C(NH_2)_3]_4Br_2SO_4$, has been characterized by dielectric, calorimetric and dilatometric methods, and its paraelectric and ferroelectric structures determined by x-ray diffraction. The crystal undergoes the first-order ferroelectric-paraelectric phase transition at $T_C=365.5$ K. The transition is driven by disordering of the SO_4^{2-} anions, but the spontaneous polarization originates essentially from the ionic displacements. The temperature dependence of the order parameter is well described by Landau's mean-field approximation. By comparing with $[C(NH_2)_3]_4Cl_2SO_4$ crystal it has been shown that the Br/Cl halogen atom exchange caused the anisotropic deformation of the crystal lattice modifying the ionic and hydrogen-bond interactions, resulting in the upward shift of the Curie point, the essential changes in the crystal phase diagram, and modified ferroelectric properties. Although the paraelectric phases of $[C(NH_2)_3]_4Cl_2SO_4$ and $[C(NH_2)_3]_4Br_2SO_4$ are isostructural in tetragonal space groups $I\bar{4}2m$, below T_C the first one becomes a two-directional ferroelectric in space group $Cmc2_1$, while the second one a one-directional ferroelectric in space group $Fmm2$. The room-temperature ferroelectricity, and the high piezoelectric response and large electric field-switchable strain, revealed in $[C(NH_2)_3]_4Br_2SO_4$, can be useful for electronic applications.

DOI: 10.1103/PhysRevB.73.134111 PACS number(s): 77.80.−e, 61.50.Ks, 77.22.−d, 65.40.−b

I. INTRODUCTION

Coherent arrangement of electric dipoles, resulting in a spontaneous electric polarization switchable over by an external electric field, is the prominent feature of ferroelectric materials. Such materials are highly desirable for applications in modern electronic devices.[1,2] Piezoelectric strain generated by ferroelectrics in the electric field is another useful effect extensively employed in actuators and sensors.[3–5] Apart from straightforward practical applications, study of ferroelectric materials is strongly motivated by basic research of condensed matter.

Recently we have reported on a new molecular-ionic crystal of tetraguanidinium dichloro-sulfate, $[C(NH_2)_3]_4Cl_2SO_4$ (hereafter $G_4Cl_2SO_4$), exhibiting ferroelectric properties at room temperature.[6] A characteristic feature of this crystal structure is its double anionic sublattice built of monovalent Cl^- and divalent SO_4^{2-} anions submerged in the sublattice of guanidinium cations. In the ferroelectric $Cmc2_1$-symmetric phase the SO_4^{2-} groups are displaced along [001] from their symmetric sites with respect to the Cl^- neighbors and the three crystallographically different guanidinium cations occupy general sites. Thus, the spontaneous polarization occurs in this crystal essentially due to the ionic displacements. The transition to the tetragonal paraelectric phase, in space group $I\bar{4}2m$, is realized through an intermediate orthorhombic phase and is driven by an order-disorder mechanism. Interestingly the reverse transition proceeds differently. On cooling the crystal in the paraelectric phase, it transforms to the metastable ferroelectric phase, and only then it slowly transforms to the initial phase. Such a behavior indicates a nearly degenerate ground state of the crystal at room temperature. The thermodynamic behavior of such a system can be easily modified in different ways because only slight changes in the crystal cohesion forces can favor one of two energetically similar phases. Properties of many materials can be tailored by altering thermodynamic conditions or chemical composition. The deuterium substitution for hydrogen in KH_2PO_4-type ferroelectrics[7] or the ferroelectricity induced by the substitution of ^{18}O for ^{16}O in quantum paraelectric $SrTiO_3$ crystal[8] pertain to the most spectacular examples. The structure-property relationships can also be modified by substituting chemically equivalent atoms, ions or molecular groups. In this report we describe a new ferroelectric material, $[C(NH_2)_3]_4Br_2SO_4$ (hereafter $G_4Br_2SO_4$), which has been obtained by the substitution of bromine for chlorine in the prototype $G_4Cl_2SO_4$. It has been shown that the Cl^-/Br^- exchange of the halogen anion results in materials with isomorphous paraelectric structures, but considerably different ferroelectric phases.

II. EXPERIMENT

Colorless and transparent crystals of $G_4Br_2SO_4$ were grown by evaporating the aqueous solution of GBr and G_2SO_4 at room temperature. In the solution the substrates were mixed in a nonstoichiometric ratio, with an excess of G_2SO_4. Calorimetric measurements were carried out by differential thermal analysis (DTA) using a homemade apparatus. The DTA runs were recorded on heating and on cooling the samples at a rate of 3 K/min. The samples for DTA studies were prepared by grinding the crystals into a fine powder. Dielectric experiments were performed on single crystals and on polycrystalline samples pressed into pellets. Gold electrodes were deposited on the large surfaces of the samples by evaporation in a vacuum. Measurements of complex electric permittivity as a function of temperature were

TABLE I. A summary of the crystal data and structure refinement for $G_4Br_2SO_4$ in the low- and high-temperature phases.

Temperature [K]	298	370
Crystal system, space group	orthorhombic, *Fmm*2	tetragonal, $I\bar{4}2m$
Unit cell dimensions [Å]: *a*	15.148(3)	10.433(1)
b	14.513(3)	10.433(1)
c	9.321(2)	9.453(2)
Volume [Å^3]	2049.2(7)	1028.9(3)
Z, calculated density [g/cm^3]	4, 1.608	2, 1.602
Absorption coefficient [mm^{-1}]	4.091	4.074
Crystal size [mm]	$0.38\times0.3\times0.25$	$0.38\times0.3\times0.25$
θ range for data collection [°]	2.69 to 25.06	2.76 to 25.02
sin θ/λ [Å^{-1}]	0.5960	0.5951
Limiting indices *h*,*k*,*l*	−18/18, −17/0, 0/11	0/12, 0/12, −11/0
Reflections collected/unique	1020/1020	546/296
Data/restraints/parameters	1020/1/115	296/0/39
Goodness of fit on F^2	1.096	1.024
Final *R*1/*wR*2 indices [$I>2\sigma_I$]	0.0410/0.1013	0.0408/0.0899
*R*1/*wR*2 indices (all data)	0.0729/0.1131	0.0805/0.1042
Largest diff. peak/hole [eÅ^{-3}]	0.453/−0.478	0.426/−0.517

carried out in the frequency range from 1 kHz to 13 MHz with a Hewlett-Packard 4192A impedance analyzer. The amplitude of the ac measuring electric field did not exceed 5 V/cm. The temperature of the samples was changed at a rate of 0.3 K/min in the vicinity of the phase transition and 0.5 K/min, elsewhere. The dielectric hysteresis loop was observed on a thin, oriented crystal plate by a Diamant–Drenck–Pepinsky bridge method,[9] at a frequency of 50 Hz.

The single-crystal x-ray diffraction studies were carried out using a KM-4 diffractometer operating with graphite-monochromated Mo $K\alpha$ radiation. The θ-2θ scan mode at variable rate, depending on the reflection intensity, was applied. The intensities were corrected for Lorentz and polarization effects, and for absorption. The unit-cell dimensions were measured as a function of temperature by least-squares fits to 30 automatically centered reflections. The crystal was heated with a nitrogen stream using an Oxford Cryosystem attachment. The temperature of the stream was stabilized within 0.1 K.

The crystal structures were solved by direct methods with SHELXS97 program[10] and refined by full-matrix least-squares method on all intensity (F^2's) data using the SHELXL97 program.[11] All the heavy atoms were refined with anisotropic temperature factors. The H atoms were located from the molecular geometry and their isotropic temperature factors U_{iso} were assumed as 1.2 times U_{eq} of their closest heavy atoms. The crystal data together with experimental and refinement details are listed in Table I, and the final atomic coordinates and equivalent temperature factors in Table II.

III. RESULTS

A. Thermal properties

The calorimetric measurements of the polycrystalline $G_4Br_2SO_4$ sample were performed in the temperature range between 120 and 400 K. The high-temperature parts of the DTA runs are plotted in Fig. 1. It is clearly seen that the substance undergoes a first-order phase transition around 365 K. At the temperature rate of 3 K/min, the onset of the anomaly was observed at (367.0 ± 0.5) K and at (363.0 ± 0.5) K, respectively, in the heating and cooling cycles. From the shape of the thermal anomaly one can infer that below the transition temperature the crystal exhibits a pre-transitional effect, which gives an additional contribution to the total entropy change associated with the transition. The results presented here allowed us to estimate only roughly this contribution as its magnitude was strongly dependent on the choice of the base line. The transition enthalpy ΔH, calculated for the base line shown as dashed line in Fig. 1, amounts to 1.52 kJ mol^{-1}. The corresponding entropy change ΔS is of 4.1 J mol^{-1} K^{-1}. The uncertainty of these thermodynamic parameters estimated by probing alternative base lines reaches 20%, much higher than the apparatus accuracy. By taking into account this uncertainty and the presence of the pre-transitional contribution, we conclude that the total entropy gain should be very close to $R\ln 2$ (where R is the gas constant). This result suggests a two-configurational disorder in the high-temperature phase of $G_4Br_2SO_4$.

B. Temperature dependence of lattice parameters

The phase transition observed in the calorimetric experiments has been confirmed by the results of dilatometric measurements shown in Fig. 2. The abrupt changes in the unit-cell dimensions at the transition temperature testify to the first-order character of the transition. A clearly anomalous thermal expansion of the crystal is seen in the low-temperature phase. The temperature behavior of parameters *a* and *b*, illustrated in Fig. 2(a), evidences that the transition

TABLE II. Atomic coordinates ($\times 10^4$) and equivalent thermal parameters ($Å^2 \times 10^3$) for $G_4Br_2SO_4$ in the orthorhombic phase at 298 K and in the tetragonal phase at 370 K. U_{eq} is defined as one third of the trace of the orthogonalized U_{ij} tensor.

	x	*y*	*z*	U_{eq}
		298 K		
Br(1)	8393(1)	7481(1)	0	61(1)
S(1)	5711(1)	5000	−66(4)	37(1)
O(1)	5155(4)	4182(4)	−277(9)	64(2)
O(2)	6478(7)	5000	−968(12)	72(3)
O(3)	5948(7)	5000	1473(11)	82(3)
C(1)	6018(7)	8063(6)	1488(11)	56(2)
N(1)	5219(5)	8248(8)	1932(10)	80(3)
N(2)	6150(9)	7451(6)	430(15)	91(4)
N(3)	6692(5)	8489(5)	2052(10)	66(2)
C(2)	7752(7)	10000	−1580(14)	52(3)
N(21)	8417(10)	10000	−665(19)	93(5)
N(22)	7421(7)	9213(6)	−2033(12)	80(3)
C(3)	9081(10)	5000	−1471()16	63(4)
N(31)	8530(10)	5000	−403(17)	85(5)
N(32)	9401(9)	4215(7)	−1944(12)	103(4)
		370 K		
S(1)	5000	5000	0	68(1)
O(1)	5476(17)	4524(17)	1180(20)	189(15)
O(2)	5000	3521(11)	0	127(6)
Br(1)	10000	5000	0	91(1)
C(1)	8145(8)	1855(8)	1500(12)	87(3)
N(1)	7686(7)	800(8)	2017(8)	119(3)
N(2)	7550(6)	2450(6)	450(14)	134(6)

occurs between the orthorhombic and tetragonal phases. The orthorhombic distortion of the structure is very profound. Worth noting is also a negative change in the crystal volume, shown in Fig. 2(b), reflecting a more densely packed crystal structure in the high-temperature phase compared to the low-temperature one.

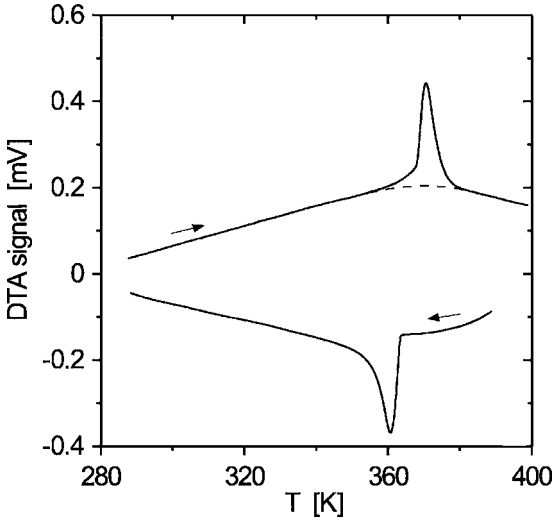

FIG. 1. DTA heating and cooling runs measured for the polycrystalline $G_4Br_2SO_4$ sample in the vicinity of the phase transition.

C. Crystal structure description

The crystal structure of $G_4Br_2SO_4$ in both low- and high-temperature phases, shown in Fig. 3, can be assumed as consisting of the lattice of guanidinium cations with voids consecutively occupied by Br^- and SO_4^{2-} anions. Thus each anion is surrounded by the guanidinium cations, and cohesion forces in this ionic crystal are dominated by the electrostatic attraction between the cations and anions. Apart from the electrostatic forces, this structure is also stabilized by hydrogen bonds between the guanidinium cations and the anions—the $NH^{\delta+}-O^{\delta-}$ and $NH^{\delta+}-Br^-$ are common types of hydrogen bonds. The size and shape of the anions are crucial for the symmetry of the crystal, as can be clearly observed by comparing the analogous crystals with different halogen anions, i.e., $G_4Br_2SO_4$ and $G_4Cl_2SO_4$. However, the structural feature of the anions being surrounded by the guanidinium cations is common for both these crystals. It can be observed for the room-temperature structure of $G_4Br_2SO_4$ that the coordination schemes of the guanidinium cations about either of the anions approximate the $\bar{4}2m$ symmetry. In the low-temperature phase the Br^- anion is located in a general position, and the SO_4^{2-} anion lies on the mirror plane perpendicular to [010]. The symmetry of the immediate vicinities of the anions is illustrated in Fig. 4. Naturally, owing to the spherical symmetry of the Br^-, only the displacements of this anion break the lattice site $\bar{4}2m$ symmetry approximated by

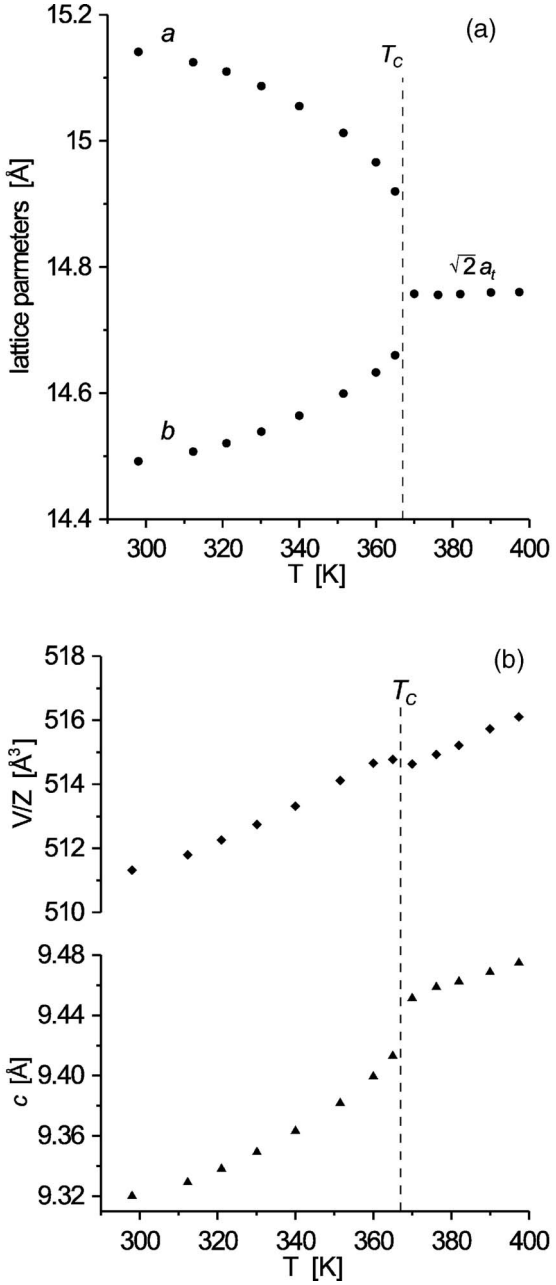

FIG. 2. Temperature dependence of the unit-cell dimensions a, b (a) and c as well as formula-unit volume V/Z (b) of $G_4Br_2SO_4$ in the orthorhombic and tetragonal phases, measured in the heating cycle of the crystal.

the surrounding of coordinating guanidinium cations. As for the SO_4^{2-} anion, apart from its displacement from the average midpoint between its coordinating guanidinium cations, also the orientation of the anion considerably diverts from the $\bar{4}2m$ symmetry approximated by the surrounding cations. It can be clearly seen in Fig. 4, that in fact one of the S-O bonds is nearly parallel to [001], which breaks the site symmetry considered. In principle, the tetrahedral SO_4^{2-} anion could change the orientation in this way that one of its three $\bar{4}$ axis passing through S1 and bisecting the O-S1-O angle be parallel to [001].

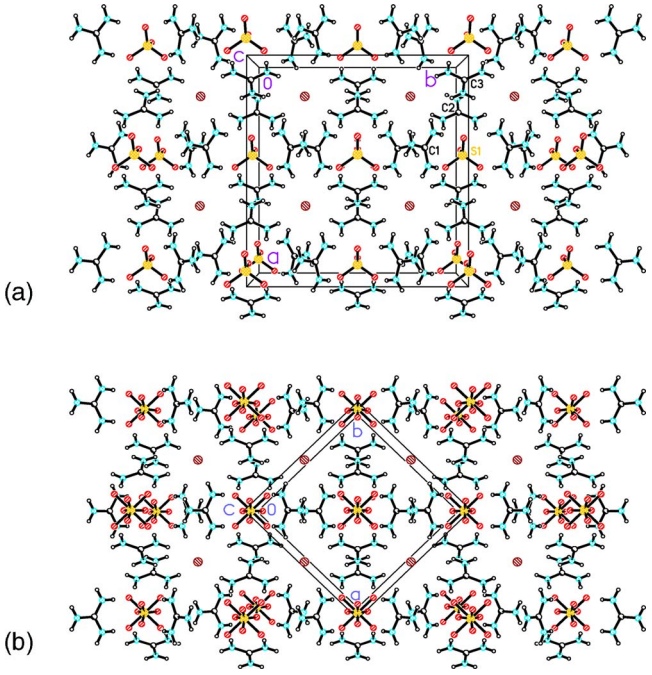

FIG. 3. (Color online) Autostereograms (see Ref. 12) of the stick-and-ball models of the $G_4Br_2SO_4$ structure in the orthorhombic ferroelectric phase (a), and in the tetragonal paraelectric phase (b).

As has been observed from calorimetric measurements, and then confirmed by the crystal structures of both low- and high-temperature phases, the $I\bar{4}2m$ symmetry of the crystal is achieved not only by small displacements and rotations of the anions and cations, but also due to the disorder of the SO_4^{2-} anions. The SO_4^{2-} groups disorder is such that the arrangement of partly occupied sites of the oxygen atoms become $\bar{4}2m$ symmetric, and the whole structure transforms to the paraelectric phase. It seems that the reason for the disordering of the anion (as opposed to the displacements) in the paraelectric phase is the bistable orientation of the anion due to the directional character of the hydrogen bonds to the

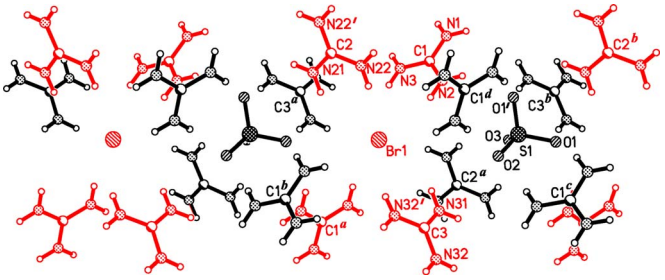

FIG. 4. (Color online) The fragment of the $G_4Br_2SO_4$ structure in the $Fmm2$ phase, showing in an autostereographic projection the surrounding of the Br^- and SO_4^{2-} anions by guanidinium cations. The guanidinium cations closest to the Br^- anion have been marked in red, and those closest to the SO_4^{2-} anion have been shown in black. In this drawing the [001] axis is vertical. The primed labels indicate the symmetry-generated atoms of the ions located on special positions, while superscripts a-d denote the ions symmetry generated to complete the closest surroundings of Br^- and SO_4^{2-}.

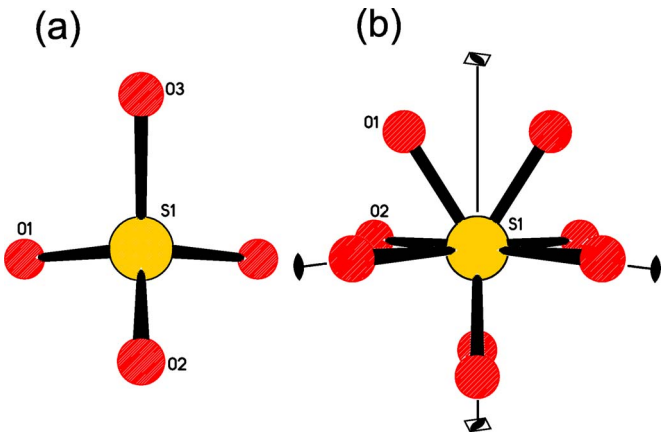

FIG. 5. (Color online) The sulphate anion in the $G_4Br_2SO_4$ structure: (a) the ordered model at 298 K, viewed in the [100] direction of the orthorhombic unit cell; and (b) the disordered model with oxygen sites half occupied at 370 K, viewed along the [110] direction of the tetragonal unit cell. In both drawings the [001] direction is vertical. In the low-temperature structure (a) atoms S1, O2 and O3 are located on the mirror plane (perpendicular to the page); and the high-temperature site (b) is $\bar{4}2m$-symmetric—of two vertical mirror planes one lies in the plane of the page and the other one is perpendicular, and the symmetry axes have been indicated.

surrounding cations. In the ferroelectric state, each of the cations with carbon atoms $C1^c$, $C1^d$ and $C3^b$ in Fig. 4 forms a pair of hydrogen bonds to a pair of oxygen atoms of the SO_4^{2-} anion. A very similar arrangement of hydrogen bonds stabilizes the layered structures of guanidinium sulfonates.[13] The fourth guanidinium (with carbon $C2^a$ in Fig. 4) does not form such a favored pair of hydrogen bonds. The SO_4^{2-} anion can reorient to form the three pairs of hydrogen bonds with another set of three guanidinium cations. Thus, at high temperature the SO_4^{2-} anion becomes activated to jump between these orientations favored by the hydrogen bonds. This explains the disorder of the anion illustrated in Fig. 5.

D. Dielectric properties

The complex electric permittivity was measured both on the pressed pellets and oriented plates cut from the single crystals. Because the crystals crack at the transition point the results obtained for these samples were characterized by a rather poor reproducibility. Therefore, we present here only the perfectly reproducible dielectric response of $G_4Br_2SO_4$ measured for the polycrystalline samples. As shown in Fig. 6(a) the temperature dependence of the real part of electric permittivity exhibits an anomaly typical of first-order paraelectric-ferroelectric phase transition, consistent with the symmetry change of the crystal from the polar orthorhombic space group $Fmm2$ to the tetragonal nonpolar space group $I\bar{4}2m$. A clear temperature hysteresis of 1.7 K was observed between the heating and cooling measurements: on heating the transition occurred at (365.5±0.2) K, while on cooling it was observed at (363.8±0.2) K. The temperature dependence of a static (or low-frequency) dielectric constant should obey the Curie–Weiss law: $\varepsilon' - \varepsilon'_\infty = C/(T-T_0)$,

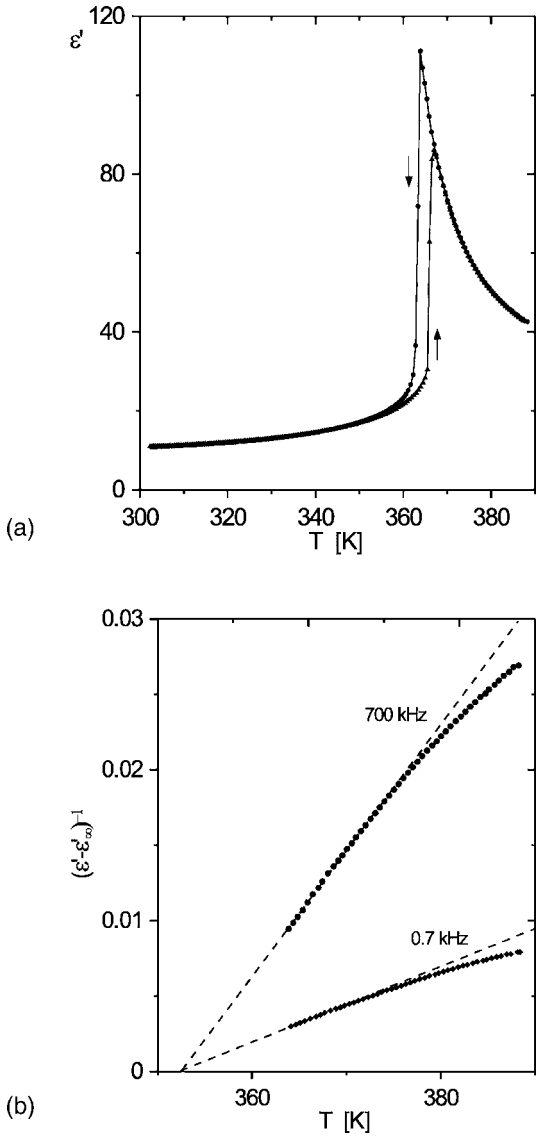

FIG. 6. Temperature dependence of the real part of electric permittivity ε' measured at 700 kHz on heating and cooling the polycrystalline sample (a); and the illustration of fulfillment of the Curie–Weiss law in the paraelectric phase (b). The dashed lines represent the best fits of the Curie–Weiss rule to the experimental data measured at 0.7 and 700 kHz on cooling the sample.

where ε'_∞ is the high-frequency electric permittivity (temperature independent), and T_0 is the Curie–Weiss temperature (for the first-order phase transitions T_0 and the Curie temperature T_C are different). Figure 6(b) presents the fittings of the Curie–Weiss law to the 0.7 and 700 kHz data measured in the paraelectric phase on cooling the sample. As clearly seen, the slopes of the fitted lines are very different for both frequencies. The low-frequency $\varepsilon'(T)$ dependence obeys the Curie–Weiss law only in a narrow temperature range of 3 K above T_C. The dashed line in Fig. 6(b), approximating a linear part of the 0.7 kHz curve, corresponds to the following parameters: $\varepsilon'_\infty = 5.5$, $C^+ = 3986$ K and $T_0^+ = 352.2$ K. The fitting procedure performed for the 700 kHz data showed that at this frequency the Curie–Weiss law is fulfilled in a wider temperature range, between T_C and T_C

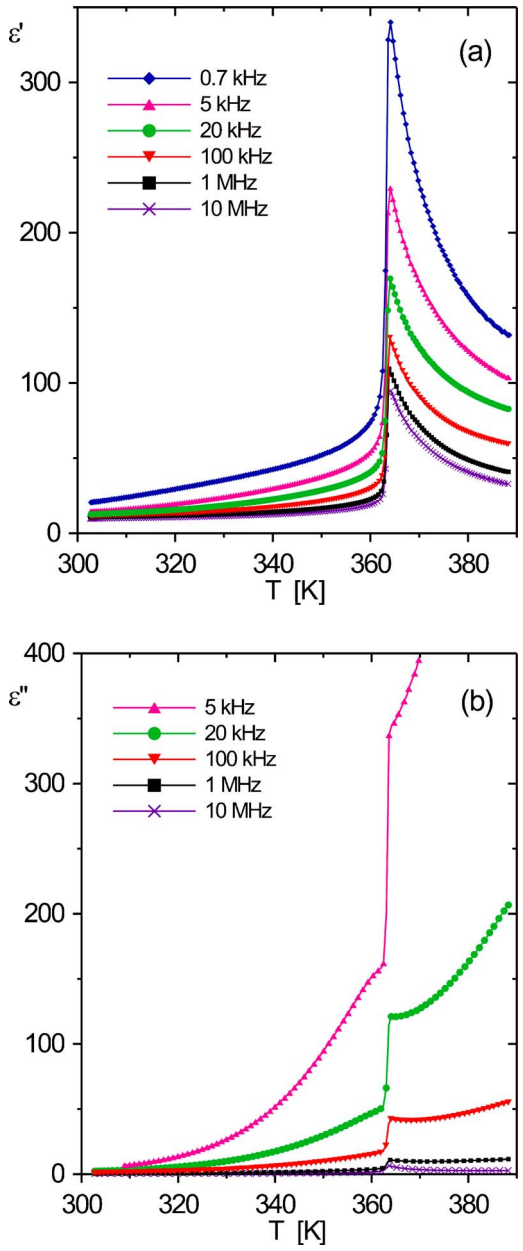

FIG. 7. (Color online) Temperature dependencies of the real (a) and imaginary (b) parts of the complex electric permittivity of $G_4Br_2SO_4$, measured at several frequencies on cooling the polycrystalline sample.

+8 K, with the parameters $\varepsilon'_\infty = 5.5$, $C^+ = 1154$ K and $T_0^+ = 352.0$ K. Large differences between the C^+ constants obtained from these fittings arise not only from the fact that the frequency of 700 kHz may not fulfil the "low-frequency" requirement. Figure 7 illustrates the frequency and temperature dependencies of the real ε' and imaginary ε'' parts of the complex electric permittivity of $G_4Br_2SO_4$. The dispersion observed in the ferroelectric phase can be ascribed both to the appearance of the ferroelectric/ferroelastic domain structure below T_C and to the effects related to the dc conductivity. The conductivity contribution is apparently reduced when the sample is cooled, and at room temperature its influence on the crystal permittivity seems to be negligible. On

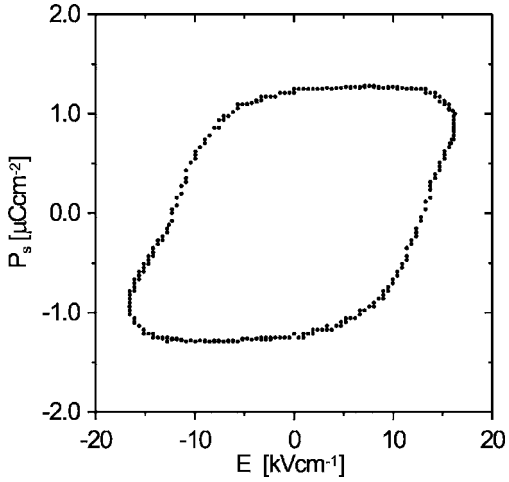

FIG. 8. The 50 Hz hysteresis loop recorded on the $G_4Br_2SO_4$ crystal at 298 K.

the other hand, the strong frequency dependence of ε' and ε'' in the paraelectric phase is caused primarily by the electric conductivity of the sample. The dielectric absorption increases suddenly at T_C, as shown in Fig. 7(b). Moreover, the low-frequency absorption rises quickly with temperature above T_C. This effect strongly influences the low-frequency electric permittivity, and hence the Curie–Weiss constant acquires an overestimated value. Therefore, from the data presented here it is possible to estimate only that C^+ is of an order of 10^3 K.

A convincing evidence of the ferroelectric properties of the low-temperature phase of $G_4Br_2SO_4$, below T_C, is provided by the ferroelectric hysteresis loop shown in Fig. 8. The 50 Hz electric field was applied along direction [001] of the *Fmm*2 phase. The loop recorded at room temperature seems to be close to saturation. The spontaneous polarization roughly estimated from the plot in Fig. 8 reaches a value of (1.3 ± 0.2) μC/cm^2. At 298 K the coercive field is relatively high and it amounts to (12.5 ± 0.5) kV/cm.

IV. DISCUSSION

In the high-temperature phase the crystal structure of $G_4Br_2SO_4$ is isosymmetric with that of its chloride analog, but the lattice translations of both crystals show clear differences. In the tetragonal phase of $G_4Br_2SO_4$ the a/c ratio amounts to 1.104, and is higher than the value of 1.068 observed for the chloride analog. So, the exchange of spherically symmetric anions of different ionic radii results in a strongly asymmetric deformation of the crystal lattice. This would indicate essential differences in the packing and in the forces acting between the ions in these crystals. Indeed, despite the evident structural proximity, the thermodynamic behavior of these compounds and their properties are very different. First of all, it is revealed in the ambient-pressure phase diagrams. It has been established that on heating the $G_4Cl_2SO_4$ crystals undergo a sequence of two successive phase transitions and on the reverse path, on cooling, they transform to the metastable, intermediate ferroelectric phase.

For $G_4Br_2SO_4$ only one clearly reversible phase transition is observed. The transition entropy change in the bromide is close to $R \ln 2$, which is consistent with the two-site disorder of the SO_4^{2-} anions in the tetragonal paraelectric phase. Much more complex disorder is observed in the high-temperature phase of the chloride analog, for which the total transition entropy gain is almost by an order of magnitude larger. In $G_4Br_2SO_4$ the ferroelectric-paraelectric phase transition takes place at temperature about 10 K higher than in $G_4Cl_2SO_4$. This is rather unexpected because the structure of $G_4Cl_2SO_4$ is more tightly packed and, therefore, the cation-anion interactions as well as the hydrogen-bonding interactions should better stabilize the low-temperature phase in this substance. The reverse situation indicates that the disordering of the SO_4^{2-} groups is mediated by the lattice mode vibrations. At room temperature the ferroelectric phases of both crystals are orthorhombic, but their space-group symmetries are different: $Cmc2_1$ and $Fmm2$, for $G_4Cl_2SO_4$ and $G_4Br_2SO_4$ respectively. The unit cells have been chosen according to the crystallographic convention and the corresponding unit-cells' dimensions are: $a_{Br}=c_{Cl}$, $b_{Br}=a_{Cl}$ and $c_{Br}=b_{Cl}$ (where the subscripts denote the chloride and bromide compounds, respectively). It is of primary importance that the ferroelectric alignment of the electric dipoles takes place along the crystallographic directions, which are nonequivalent in both crystals. In $G_4Br_2SO_4$ the spontaneous polarization P_s occurs along [001] of the prototypic tetragonal phase, while in $G_4Cl_2SO_4$ it is observed in the plane perpendicular to [001], along the directions [110] or $[1\bar{1}0]$. This indicates that we deal with the one- and two-directional ferroelectrics, respectively. Thus one can expect that the microscopic origin of ferroelectric polarization is different in both these compounds. Using the crystallographic data collected in Table II it is easy to calculate the relative displacement of the Br^- and SO_4^{2-} anionic sublattices along [001]. This displacement is only of 0.062 Å, much less than 0.267 Å of the analogous effect along the ferroelectric axis in $G_4Cl_2SO_4$. The small relative displacements of the monovalent and divalent ions can be a primary reason for the lower value of P_s in the bromide compound. The contribution to the spontaneous polarization arising from the ionic displacements in the $G_4Br_2SO_4$ ferroelectric structure was modeled using a simple point-charge approximation. The charges of the ions were assumed on their central atoms. The three crystallographically different guanidinium cations are displaced in different ways from their symmetric sites in the paraelectric phase and therefore they produce different contributions to the total P_s. Namely, the eight cations $G(1)$ (the numbering of the cations is consistent with the labels of the carbon atoms in Table II) give the contribution $P_1=-22.828\ \mu C/cm^2$, the sense of which is the opposite to the contributions of the four cations $G(2)-P_2=11.103\ \mu C/cm^2$, and of the four cations $G(3)-P_3=12.402\ \mu C/cm^2$. The resulting polarization P_s(calc) amounts to $0.68\ \mu C/cm^2$. This value well agrees with the value of P_s determined experimentally by the hysteresis loop method, testifying to the essentially displacive nature of spontaneous polarization in $G_4Br_2SO_4$. Moreover, the model calculations indicate that in the bromide crystal the displacive contribution to P_s is much lower than in its chloride analog,[6] for which P_s(calc) $=11.02\ \mu C/cm^2$. Analysis of the room-temperature structure of $G_4Br_2SO_4$ shows that the ions in the crystal lattice are slightly distorted from their ideal triangular and tetrahedral symmetric geometries. These distortions can result in dipole moments and thus, in the additional contributions to P_s. Similar effects can be associated with the charge distribution along the hydrogen bonds.

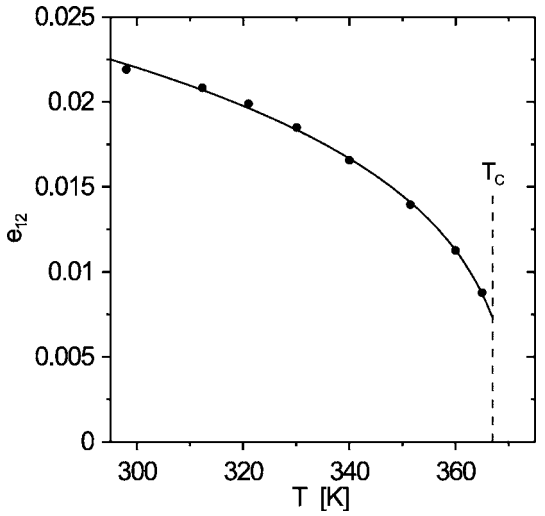

FIG. 9. Temperature dependence of the spontaneous shear strain e_{12} in $G_4Br_2SO_4$, calculated from the data shown in Fig. 2. The solid line represents theoretical behavior of the order parameter described by Equation (2).

According to the symmetry change the phase transition in $G_4Br_2SO_4$ can be classified, in Aizu's notation,[14] as belonging to the $\bar{4}2mFmm2$ species. The group-subgroup relation implies that the transition is both ferroelectric and ferroelastic.[15] Thus, in the low-temperature phase two ferroelectric domains with P_s of the opposite sense, and two ferroelastic domains characterized by different orientation states, can be formed. For such type of phase transitions the spontaneous strain tensor has only one nonzero component e_{12}, linearly coupled to P_s. Therefore, both these parameters can serve, on equal terms, as macroscopic order parameters. The spontaneous shear strain can be easily calculated from the temperature dependence of the lattice parameters (Fig. 2) according to the formula[16]

$$e_{12} = (a-b)/(a+b). \tag{1}$$

The temperature behavior of e_{12} is shown in Fig. 9. This temperature dependence can be described in the Landau's mean-field approximation.[17,18] For a first-order phase transition the simplest expansion of the Landau free energy assumes the following form:

$$F = F_0 + g_2\eta^2 + g_4\eta^4 + g_6\eta^6, \tag{2}$$

where F_0 is the free energy of the high-temperature phase and η is the order parameter. When assuming that in the vicinity of the critical temperature T_0 the coefficient g_2 changes linearly with temperature, $g_2=\alpha(T-T_0)$, the temperature dependence of the order parameter is given by

$$\eta = A\{[1 + B(T_0 - T)]^{1/2} - 1\}^{1/2}, \quad (3)$$

where $A=(-g_4/3g_6)^{1/2}$ and $B=3\alpha g_6/(g_4)^2$. The goodness of fit of the experimentally measured values of e_{12} to the function in Eq. (3) is of 0.999. The solid line in Fig. 9 represents the best fit obtained with the fitting parameters: $A=0.0137$, $B=0.1672$ K^{-1} and $T_0=370.9$ K. As is evident from the plot in Fig. 8 the mean-field approximation holds very well in a wide temperature range.

The spontaneous shear strain e_{12}, occurring in the plane perpendicular to the ferroelectric axis, is coupled to the spontaneous polarization P_s by a linear expression[19]

$$e_{12} = \frac{1}{2} g_{36} P_s, \quad (4)$$

where g_{36} is a piezoelectric coefficient. Taking into account that the piezoelectric modulus $d_{36}=\varepsilon_0 \varepsilon' g_{36}$ (ε_0 denotes the electric permittivity of vacuum) it is easy to estimate roughly the room-temperature value of d_{36}. Using Eq. (4) and assuming $\varepsilon'=8$ (the value measured at 100 kHz for the single-crystal sample, at 298 K) and $P_s=1.3$ μC/cm^2 we obtained $d_{36}=240$ pC/N. This is a very high value, by an order of magnitude higher than that in KH_2PO_4, the prototypical hydrogen-bonded crystal. It is also worth noting that the strong orthorhombic deformation of the $G_4Br_2SO_4$ crystal lattice in the ferroelectric phase implies a large electro-strain effect due to the ferroelectric domains switching. The change in the polarization direction requires the exchange of the crystallographic directions a and b, resulting in the 2.2% macroscopic shape deformation of the crystal. As has been recently demonstrated, such an effect, together with an appropriate doping of the crystal, can be employed for the new generation actuators.[20]

V. CONCLUSIONS

The substitution of Br^- for Cl^- in the prototypical ferroelectric guanidinium salt $G_4Cl_2SO_4$ results in the isomorphous crystal of $G_4Br_2SO_4$, which also exhibits room-temperature ferroelectricity. The increase in the radius of the halogen anion leads to the anisotropic expansion of the crystal lattice, modifying the crystal cohesion forces: the ionic and hydrogen-bonding interactions. In consequence, the crystal structure acquires new features different from those of its prototype. Thus, at ambient pressure, $G_4Br_2SO_4$ undergoes only a single phase transition between the orthorhombic ferroelectric and tetragonal paraelectric phases, and its room-temperature phase does not exhibit any metastable properties or energetically degenerated states, as observed for $G_4Cl_2SO_4$. Moreover, in $G_4Br_2SO_4$ the spontaneous polarization occurs only along one direction parallel to the tetragonal [001] axis, whereas two directions perpendicular to [001] are permissible for P_s in $G_4Cl_2SO_4$. Although both in $G_4Br_2SO_4$ and $G_4Cl_2SO_4$ the transition to the paraelectric phase is driven by stochastic motions of the SO_4^{2-} tetrahedra, their isosymmetric high-temperature structures show clearly a different degree of disordering.

The phase transition in $G_4Br_2SO_4$ is similar in many aspects to that in the well known KH_2PO_4 ferroelectric: (i) the crystals belong to the same $\bar{4}2mFmm2$ species, (ii) their paraelectric-ferroelectric phase transitions involve the order-disorder contributions, but their spontaneous polarizations originate essentially from the ionic displacements, (iii) the pressure dependences of their Curie–Weiss temperatures are characterized by the negative pressure coefficients dT_C/dp (for $G_4Br_2SO_4$ this can be inferred from the negative change of the crystal volume at T_C), (iv) in both these crystals P_s is generated parallel to the tetragonal direction [001] and it is coupled linearly to the shear strain occurring in the plane perpendicular to [001]. However, it should be stressed that the shear strain in $G_4Br_2SO_4$ is several times larger in magnitude than that in KH_2PO_4, and besides it exists, together with ferroelectric polarization, at room temperature. Materials with ferroelectric and piezoelectric properties in the room-temperature range, like those in $G_4Br_2SO_4$, are of special interest owing to their potential applications.

[1] M. Lines and A. M. Glass, *Principles and Applications of Ferroelectric and Related Materials* (Oxford University Press, Oxford, 1979).
[2] J. F. Scott, *Ferroelectric Memories* (Springer, Berlin, 2000).
[3] K. Uchino, *Piezoelectric Actuators and Ultrasonic Motors* (Kluwer, Boston, 1996).
[4] S. E. Park and T. R. Shrout, J. Appl. Phys. **82**, 1804 (1997).
[5] R. Service, Science **275**, 1878 (1997).
[6] M. Szafrański, Phys. Rev. B **72**, 054122 (2005).
[7] F. Jona and G. Shirane, *Ferroelectric Crystals* (Dover, New York, 1993).
[8] M. Itoh, R. Wang, Y. Inaguma, T. Yamaguchi, Y.-J. Shan, and T. Nakamura, Phys. Rev. Lett. **82**, 3540 (1999).
[9] H. Diamant, K. Drenck, and R. Pepinsky, Rev. Sci. Instrum. **22**, 30 (1957).
[10] G. M. Sheldrick, SHELXS97, program for solution of crystal structures (University of Göttingen, Göttingen, Germany, 1997).
[11] G. M. Sheldrick, SHELXL97, program for crystal structure refinement (University of Göttingen, Göttingen, Germany, 1997).
[12] A. Katrusiak, J. Mol. Graphics Modell. **19**, 363 (2001).
[13] V. A. Russell, M. C. Etter, and M. D. Ward, J. Am. Chem. Soc. **116**, 1941 (1994).
[14] K. Aizu, J. Phys. Soc. Jpn. **27**, 387 (1969).
[15] V. Janovec, V. Dvorak, and J. Petzelt, Czech. J. Phys., Sect. B **25**, 1362 (1975).
[16] J. Sapriel, Phys. Rev. B **12** 5128 (1975).
[17] L. D. Landau and E. M. Lifshitz, *Statistical Physics* (Pergamon, Oxford, 1969).
[18] J.-C. Toledano and P. Toledano, *The Landau Theory of Phase Transitions* (World Scientific, Singapore, 1987).
[19] J. Kobayashi, Y. Uesu, I. Mizutani, and Y. Enomoto, Phys. Status Solidi A **3**, 63 (1970).
[20] X. Ren, Nat. Mater. **3**, 91 (2004).